Massive Neutrinos in a Λ Cold Dark Matter Cosmology

Dana Simard,[1,*] Ue-Li Pen,[2,†] and P. Daniel Meerburg[2,‡]

[1] *Department of Astronomy and Astrophysics, University of Toronto, 50 St. George St., Toronto, ON M5S3H8, Canada*

[2] *Canadian Institute for Theoretical Astrophysics, University of Toronto, 60 St. George St., Toronto, ON M5S 3H8, Canada*

(Dated: September 16, 2015)

We present a fast, semi-linear treatment of massive neutrinos in a fully cosmological ΛCDM universe. Due to the clustering of cold dark matter, a fully linear treatment of the cosmology is insufficient to model massive neutrino behaviour. However, numerical simulations of neutrinos are hindered by high Poisson noise and long computation times. Many hybrid methods of including neutrinos in numerical simulations have been proposed, but these neglect the neutrino response to non-linear cold dark matter and therefore are unable to resolve non-linear neutrino structure. We treat neutrinos as a linear fluid in a non-linear gravitational potential determined from N-body simulations of cold dark matter. Under the approximation that the gravitational potential is dominated by cold dark matter, we use unequal-time cross correlators of the numerical cold dark matter power spectrum as a measure of the gravitational potential. We then evolve neutrinos under the fluid approximation in this fully non-linear potential. Due to the low computational cost of this method, it lends itself well to studies of non-linear neutrino behaviour, especially for low mass neutrinos or those with properties that are difficult to include in numerical simulations. Understanding non-linear neutrino behaviour will provide better predictions for relic neutrino direct detection experiments, which may provide insight into both neutrinos and the early universe they probe in the near future.

I. INTRODUCTION

Neutrinos remain one of the more elusive particles in the standard model despite extensive research in both the particle and cosmological physics communities. Neutrino oscillation experiments have determined the mass differences between species of neutrinos ($\Delta m^2_{21} \approx 7.6\ 10^{-5}$ eV^2 and $\Delta m^2_{31} \approx 2.4\ 10^{-3}$ eV^2) (see [1] for a recent analysis), constraining the sum of the neutrino masses to $\sum m_\nu \gtrsim 0.05$ eV, while double-beta decay experiments provide a complimentary constraint of $\sum m_\nu \lesssim 0.2$ eV (see [2] for a recent review). Meanwhile, since neutrinos affect structure formation (see, for example, [3] and [4]), cosmological observations can provide insight into neutrino properties. Cosmic microwave background (CMB) lensing observations from the Planck satellite have constrained the sum of the neutrino masses to $\sum m_\nu < 0.24$ eV (95% confidence limits) [5]. When these observations are combined with the matter power spectrum of large scale structure from the WiggleZ survey, an even lower limit of $\sum m_\nu < 0.18$ eV (95% confidence) is obtained [6]. While these experiments and observations have placed constraints on the masses of the neutrino species, many questions including the absolute masses and mass hierarchy of neutrino species as well as whether or not the neutrino is a Majorana particle, remain unanswered. In the future, some of these answers may be provided by direct detection of the cosmic neutrino background. As the cosmic neutrino background is much older than the CMB (neutrinos and photons decoupled around 1 MeV and 0.25 eV respectively [7]), observations of the cosmic neutrino background could also provide insight into the physics of the early universe. The Princeton Tritium Observatory for Light, Early-Universe, Massive-Neutrino Yield (PTOLEMY), currently in the research and design phase, will search for relic neutrinos through neutrino capture by tritium and thereby constrain the neutrino masses. If neutrino clustering is ignored, 9 - 10 detections of relic neutrinos are expected from PTOLEMY per year [8]. However, to better predict PTOLEMY results and their dependence on, for example, neutrino mass, we require an understanding of neutrino clustering, and how that might affect the neutrino sample available to PTOLEMY.

One challenge to studies of cosmic neutrinos is modelling the cosmic neutrino background. To study the effects of neutrinos on large scale structure formation, one can evolve a grid-based neutrino density field simultaneously with an N-body simulation of cold dark matter (CDM) (*e.g.* [9]). However, these studies are in general unable to resolve non-linear neutrino structure. An alternative is to include neutrinos as distinct particles in N-body simulations [10, 11]. These particle-based simulations of neutrinos have indicated that a purely linear cosmology is insufficient to describe the evolution of the cosmic neutrino background: Both the neutrino matter and velocity power spectra are underpredicted by linear theory [11, 12]. However, because neutrinos have high velocity dispersions, N-body simulations including neutrinos as separate particles are hindered by

*Electronic address: simard@cita.utoronto.ca
†Electronic address: pen@cita.utoronto.ca
‡Electronic address: meerburg@cita.utoronto.ca

high Poisson noise. The common solution to high Poisson noise, increasing the number of particles simulated, greatly increases the computation time, which is already large due to the small time step required to resolve the rapidly moving neutrinos [9, 12, 13]. This makes performing many of these simulations both costly and time-consuming. Because of this, using N-body simulations to perform a parameter-space study of the consequences of various neutrino properties is currently impractical, especially at low masses.

To improve upon hybrid N-body simulations of neutrinos, [12] initially evolve neutrinos in linear theory on a grid, and convert them to particles at a later time. However, this method still fails to capture the neutrino response to a non-linear gravitational potential at early times. [14] take a different approach and include the full non-linear gravitational potential contributed by neutrinos and CDM when evolving the neutrino grid, thereby including the linear neutrino response to the non-linear gravitational potential. However, when they compute the gravitational potential, [14] neglect the temporally changing phase of the matter density field.

In this work, we study the evolution of the cosmic neutrino background in a ΛCDM cosmology using a combination of N-body simulations and analytical methods. We work in the approximation that the gravitational potential is due entirely to CDM. As a result, while we include CDM in the numerical simulations in order to accurately capture non-linear CDM self-interactions, we omit the neutrinos from these simulations, avoiding the complications of N-body simulations of neutrinos described above. As the physical density of neutrinos is only a fraction of that of CDM ($\Omega_\nu = 0.002$ for $\sum m_\nu = 0.2$ eV, $\Omega_{cdm} = 0.26$ [15]), this seems a reasonable approximation. [9, 12] find that at wavenumbers $k \gtrsim 0.1$ h Mpc^{-1}, the matter power spectrum is reduced by 1.25% when neutrinos with $\sum m_\nu = 0.6$ eV are included in simulations. [12] note that this effect on the matter power spectrum scales with $\sum m_\nu$. Therefore, at the neutrino masses considered in this work $\left(\sum m_\nu \leq 0.2 \text{ eV}\right)$, we expect simulations without neutrinos to reproduce the CDM power spectrum to within a percent.

From the CDM simulations, we record the gravitational potential in the form of unequal-time CDM power spectra. Including unequal-time as well as equal-time power spectra allows us to extract multiple modes of the gravitational potential, as discussed in Section III B, preserving information on phase differences between the gravitational potential fields at different redshifts. We then approximate neutrinos as a fluid with a finite sound speed driven by the CDM gravitational potential. The validity of this treatment will be discussed in Section II B. Throughout this work, we also apply this method to a fluid approximation of CDM. Although we do not expect to improve upon a linear treatment of CDM, as the fluid approximation is not applicable on non-linear CDM scales, this serves both as a monitor of the accuracy of our semi-linear method and as an analysis of the effects of subordinate gravitational modes on CDM.

The remainder of this report is organized as follows: In Section II we discuss the validity of the fluid treatment of both neutrinos and CDM and introduce the fluid equations used in this work. In Section III we give further details of the numerical methods used in this analysis. In Section IV we present the results of the N-body simulations and compare them to the Cosmic Linear Anisotropy Solving System (CLASS) [16]. In Sections V and VI, we present and discuss the semi-linear neutrino and CDM density and velocity power spectra, respectively. Then, in Section VII, we explore the possibility of including non-linear terms in the fluid equations used in the semi-linear analyses. Finally, we conclude by considering future prospects of this work in Section VIII.

II. THEORY

Within this work, we use fluid approximations of both CDM and neutrinos to calculate the linear responses of these species to a non-linear gravitational potential. In this section we first discuss the validity of such a treatment for CDM (Section II A) and neutrinos (Section II B). We then present the fluid equations relevant to this work and derive the forms used throughout this report (Section II C).

A. Fluid approximation of cold dark matter

At times in this work, we treat CDM as a pressureless fluid. This is not strictly correct even on large scales and at early times: In a fluid we expect collisions to distribute energy between particles, so that proximal particles follow a Maxwellian velocity distribution with a well-defined mean, providing an unambiguous velocity field. Because CDM is collisionless, this process does not occur. However, at early times, we expect deviations from the Hubble flow to be very small, so that a velocity field may still be defined. As time progresses, we expect both that collisions will become more important and that CDM will gain an appreciable velocity dispersion, requiring a more complex treatment, such as N-body simulations or the Press-Schechter formalism, to accurately model the behaviour on non-linear scales of $k \gtrsim 0.1$ [7, 17, 18]. It is for this reason that we use numerical simulations to capture the non-linear behaviour of the gravitational potential sourced by CDM. However, we find that reconstructing the CDM behaviour using a fluid treatment provides valuable insight into both the accuracy of our semi-linear method and the effects of the changing gravitational potential phase on CDM.

B. Fluid approximation of massive neutrinos

A fluid treatment of massive neutrinos may be less intuitive than the treatment of CDM as a collisionless fluid. At early times, neutrinos possess a large velocity dispersion, while at late times massive non-relativistic neutrinos are collisionless, and therefore not a fluid. In spite of this, neutrinos have been treated as a fluid in various works over the last few decades (*e.g.* [19]; [20]).

There is reason to believe that a fluid approximation of neutrinos is reasonable. When the velocity dispersion of neutrinos is low enough, a fluid approximation may be applicable just as it is for CDM. Only recently has the validity of such an approximation been examined in detail. [21] examine the fluid approximation of non-relativistic massive neutrinos and find that it results in an error in the neutrino density and velocity perturbations of less than 25% (compared to the full Boltzmann treatment) for 0.05 eV to 0.5 eV neutrinos at wavenumbers $k \leq 0.4$ h Mpc^{-1} and at redshifts $z \leq 10$. They find that in this non-relativistic regime, the approximation is best at high masses and late redshifts, as expected: As shown later in this section, the velocity dispersion of neutrinos is inversely proportional to the scalefactor and the neutrino mass. [22] perform a more comprehensive study of the validity of a fluid approximation applied to neutrinos; they study the effects on the CMB and matter power spectra of fluid approximations of relativistic and non-relativistic neutrinos over a mass range of 0.001 eV to 1 eV and find that the fluid approximation is accurate to the percent level on scales $k < 1$ h Mpc^{-1}.

A fluid treatment of neutrinos is more informative than the correct full treatment of the Boltzmann hierarchy, as the continuity and Euler equations are more easily interpreted than an infinite system of equations. It is for this reason and the simplicity of implementing the fluid equations that we adopt a fluid approximation of neutrinos in this work.

When we represent neutrinos as a fluid, we must account for their finite velocity dispersion. This dispersion resists structure formation, and therefore may be approximated by a pressure or sound speed. For non-relativistic neutrinos, the sound speed, c_s, is related to the velocity dispersion, σ_v, by [21]:

$$c_s^2(t) = \frac{\delta P(k,t)}{\delta \rho(k,t)} \approx \frac{5}{9}\sigma_v^2(t) \; . \tag{1}$$

Neutrinos become non-relativistic when the momentum contribution to their energy falls below that of their mass, m_ν. [21] show that the redshift at which this occurs, z_{nr}, is given by:

$$1 + z_{nr} \approx 1890 \left(\frac{m_\nu}{1\text{eV}}\right) . \tag{2}$$

In this work, we consider neutrino masses of 0.1 eV and 0.2 eV. Therefore, at redshifts $z \lesssim 100$ the neutrinos we consider are in the non-relativistic limit and can be characterized by the sound speed in Equation (1).

Recall that the velocity dispersion is given by:

$$\sigma_v^2 =< v^2 >= \frac{1}{a^2 m_\nu^2} < q^2 > \; , \tag{3}$$

where q is the comoving non-relativistic momentum of the neutrinos and a is the scalefactor. Since the shape of the neutrino distribution function does not change after decoupling (which occurs when neutrinos are relativistic), even non-relativistic neutrinos follow the relativistic Fermi-Dirac distribution function:

$$f_o(q) = \frac{1}{\mathrm{e}^{\epsilon/aT_\nu} + 1} \; , \tag{4}$$

where ϵ is the energy, $\epsilon = \sqrt{q^2 + m^2 a^2} \approx q$ in the non-relativistic limit, and T_ν is the temperature of the neutrino distribution. After decoupling, the temperature decreases due only to the expansion of the universe so that aT_ν remains constant. This means that we may replace aT_ν in Equation (4) with $a_0 T_{\nu,0}$, the value today, which is related to the cosmic microwave background temperature, $T_{\gamma,0}$ by:

$$\frac{T_{\nu,0}}{T_{\gamma,0}} = \left(\frac{4}{11}\right)^{1/3} . \tag{5}$$

See Appendix A for a derivation of this relation.

With Equations (4) and (5), the following expression for the velocity dispersion can be derived, as detailed in Appendix B:

$$\sigma_v^2(t) = \frac{1}{a^2(t)\, m_\nu^2} 15 \frac{\zeta(5)}{\zeta(3)} \left(\frac{4}{11}\right)^{2/3} T_{\gamma,0}^2 \; , \tag{6}$$

where ζ is the Riemann zeta function. Combining this with Equation (1) gives the following expression for the sound speed:

$$c_s^2(t) \approx \frac{5}{9} \frac{1}{a^2(t)\, m_\nu^2} 15 \frac{\zeta(5)}{\zeta(3)} \left(\frac{4}{11}\right)^{2/3} T_{\gamma,0}^2 \; . \tag{7}$$

C. The fluid equations

Approximating neutrinos and CDM as fluids allows us to use the fluid equations. In this work, the continuity equation (8), the Euler equation (9), and Poisson's equation (10) will be of particular importance. The continuity equation, an expression of mass conservation, may be written as:

$$\frac{\partial \rho}{\partial t} + \nabla \cdot (\rho \mathbf{v}) = 0 \; , \tag{8}$$

where ρ is the density of the fluid, t is the physical time and $\mathbf{v}$ is the velocity of the fluid, $\frac{\partial \mathbf{r}}{\partial t}$. Both ρ and $\mathbf{v}$ depend on position $\mathbf{r}$ and time t. The Euler velocity equation for momentum conservation has the form:

$$\frac{\partial \rho \mathbf{v}}{\partial t} + (\mathbf{v} \cdot \nabla)\rho \mathbf{v} + \nabla P_T = 0 \; , \tag{9}$$

where P_T is the total pressure experienced by the fluid, including both the gravitational pressure and the outward fluid pressure. Finally, Poisson's equation for the gravitational potential, Φ, may be written:

$$\nabla^2\Phi = 4\pi G\rho \ , \tag{10}$$

where ρ is the total density and G is the gravitational constant. Note also that:

$$\nabla P_g = \rho g = -\rho\nabla\Phi \ , \tag{11}$$

where P_g is the pressure due to gravity, so that we may rewrite Equation (9) as:

$$\frac{\partial\rho\mathbf{v}}{\partial t} + (\mathbf{v}\cdot\nabla)\rho\mathbf{v} + \nabla P = \rho\nabla\Phi \ , \tag{12}$$

where P now excludes the gravitational pressure.

To attain the form of these equations used in this work, some simplifying assumptions will be made. First, we assume that the flows of interest are incompressible, or that the density of the fluid is constant within an infinitesimal volume element moving with the fluid. Under this assumption, the continuity equation remains unchanged, but the Euler Equation, Equation (12), simplifies to:

$$\frac{\partial\mathbf{v}}{\partial t} + (\mathbf{v}\cdot\nabla)\mathbf{v} + \frac{\nabla P}{\rho} = \nabla\Phi \ . \tag{13}$$

For ease of interpretation and ease of integration with the N-body simulations used in this work, we desire equations in comoving spatial coordinates, $\mathbf{x}$, related to the physical coordinates, $\mathbf{r}$, by:

$$\mathbf{r} = a(t)\mathbf{x} \ . \tag{14}$$

In comoving coordinates, we may decompose the velocity field $\mathbf{v}$ into the Hubble flow and a peculiar velocity:

$$\mathbf{v}(\mathbf{r}(t),t) = H(t)\mathbf{r}(t) + \mathbf{u}\left(\frac{\mathbf{r}}{a},t\right) \ , \tag{15}$$

where $H(t) = \frac{\dot{a}}{a}$ is the Hubble parameter. As the transformation to comoving coordinates is detailed by many authors (*e.g.* [7, 23, 24]), we reproduce only the major steps here.

As we are changing the spatial coordinates, we must also transform the derivative with respect to t from one during which $\mathbf{r}$ is held constant to one during which $\mathbf{x}$ is held constant via the relation:

$$\left(\frac{\partial}{\partial t}\right)_{\mathbf{r}} = \left(\frac{\partial}{\partial t}\right)_{\mathbf{x}} + \left(\frac{\partial\mathbf{x}}{\partial t}\right)_{\mathbf{r}}\nabla_x \ , \tag{16}$$

which in this case reduces to:

$$\left(\frac{\partial}{\partial t}\right)_{\mathbf{r}} = \left(\frac{\partial}{\partial t}\right)_{\mathbf{x}} - \frac{\dot{a}}{a}\mathbf{x}\cdot\nabla_x \ , \tag{17}$$

where

$$\nabla_{\mathbf{r}} = \frac{\nabla_{\mathbf{x}}}{a} \ , \tag{18}$$

from Equation (14). Using Equation (17), we can rewrite Equation (8) (after some manipulation) as:

$$\frac{\partial\rho}{\partial t} + 3\frac{\dot{a}}{a}\rho + \frac{1}{a}\nabla\cdot(\rho\mathbf{u}) = 0 \ , \tag{19}$$

where all derivatives are now with respect to comoving coordinates $(\mathbf{x},t)$.

We can further simplify the continuity equation by writing the density as a perturbation, $\delta(\mathbf{x},t)$, around a spatially averaged density, $\bar{\rho}(t)$: $\rho(\mathbf{x},t) = (1+\delta(\mathbf{x},t))\bar{\rho}(t)$. From the continuity equation for the homogenous mass density, $\frac{d}{dt}(\bar{\rho}a^3) = 0$, we find $\bar{\rho} \propto a^{-3}$, so that $\frac{\partial\bar{\rho}}{\partial t} = -3\bar{\rho}\frac{\dot{a}}{a}$. Using these relations, Equation (19) becomes:

$$\frac{\partial\delta}{\partial t} + \frac{1}{a}\nabla\cdot((1+\delta)\mathbf{u}) = 0 \ . \tag{20}$$

Note that $\mathbf{u}$ is already a perturbative velocity about the Hubble flow. After transforming to comoving coordinates and writing the density as a perturbation about the mean, Equation (12) becomes:

$$\frac{\partial(\dot{a}\mathbf{x}+\mathbf{u})}{\partial t} + \frac{\dot{a}}{a}\mathbf{u} + \frac{\mathbf{u}\cdot\nabla}{a}\mathbf{u} + \frac{\nabla P}{a\rho} = \frac{\nabla\Phi}{a} \ . \tag{21}$$

From the Poisson equation, the gravitational potential may be written as:

$$\Phi(\mathbf{r},t) = \left(\frac{2\pi}{3}G\bar{\rho} - \frac{\Lambda}{6}\right)|\mathbf{r}|^2 + \phi(\mathbf{x},t) = \frac{\ddot{a}a}{2}|\mathbf{x}|^2 + \phi(\mathbf{x},t) \ , \tag{22}$$

where ϕ is the gravitational potential sourced by perturbations to the homogeneous density. As mentioned in Section I, we assume that ϕ may be approximated as the gravitational potential sourced by CDM density perturbations only. (Note that in the rest of this report, we will use the subscripts c and ν to label attributes of CDM and neutrinos respectively.) ϕ_c may be related to the density perturbations, δ_c, by:

$$\nabla^2\phi_c(\mathbf{x},t) = 4\pi G a^2\overline{\rho_c}(t)\delta_c(\mathbf{x},t) = \frac{3H^2(t)a^2(t)}{2}\delta_c(\mathbf{x},t) \ . \tag{23}$$

This allows us to write Equation (21) as:

$$\frac{\partial(\dot{a}\mathbf{x}+\mathbf{u}_i)}{\partial t} + \frac{\dot{a}}{a}\mathbf{u}_i + \frac{\mathbf{u}_i\cdot\nabla}{a}\mathbf{u}_i + \frac{\nabla P_i}{a\rho_i} = \ddot{a}\mathbf{x} + \frac{\nabla\phi_c}{a} \ , \tag{24}$$

where $i = c,\nu$ for CDM and neutrinos respectively.

It is easy to verify that a homogeneous and isotropic distribution is a solution to these equations. We can expand around this solution by considering deviations from $\mathbf{u}_i = 0$ and from $\rho_i = \overline{\rho_i}$, again using $\rho_i = \bar{\rho}_i(1+\delta_i)$:

$$\frac{\partial\mathbf{u}_i}{\partial t} + \frac{\dot{a}}{a}\mathbf{u}_i + \frac{\mathbf{u}_i\cdot\nabla}{a}\mathbf{u}_i + \frac{\nabla P_i}{a\bar{\rho}_i(1+\delta_i)} = \frac{\nabla\phi_c}{a} \ . \tag{25}$$

Now that we have both the Euler and the continuity equation in comoving coordinates, we can further simplify the equations by linearizing them. By assuming

that any terms of second order or higher in the perturbation (*i.e.*, in δ or $\mathbf{u}$) are negligible, we arrive at the following forms for the continuity equation (26) and the Euler equation (27):

$$\frac{\partial \delta_i}{\partial t} + \frac{1}{a}\nabla \cdot \mathbf{u_i} = 0 \ , \tag{26}$$

and

$$\frac{\partial \mathbf{u_i}}{\partial t} + \frac{\dot{a}}{a}\mathbf{u_i} + \frac{\nabla P}{a\overline{\rho_i}} = \frac{1}{a}\nabla \phi_c \ . \tag{27}$$

These are the forms of the fluid equations used in this work.

III. METHODS

As mentioned in Section I, the semi-linear analysis employed in this work requires that we first run N-body simulations of CDM to measure the gravitational potential sourced by CDM density perturbations. We then analyze the responses of CDM and neutrinos to this gravitational potential using the fluid approximation. In Section III A, we will give an overview of the simulations used in this work, while in Section III B we will discuss the use of unequal-time power spectra as a measure of the CDM density perturbations and therefore of the gravitational potential. We will leave the calculation of the CDM and neutrino responses to this potential to Sections V and VI.

A. Numerical simulations

We use the publicly available code CUBEP^{3}M [25] to run N-body simulations of CDM in a ΛCDM cosmology on the SciNet General Purpose Cluster (GPC) [26]. CUBEP^{3}M is a high performance, cosmological N-body code that solves Poisson's equation over a two-level mesh using a particle-mesh scheme, and incorporates particle-particle interactions within the smaller mesh. This code is an improvement on its predecessors PMFAST [27] and CUBEPM, and has been used to investigate many cosmological phenomena, including the kinetic Sunyaev-Zel'dovich (kSZ) effect [28, 29], reionization [30, 31], and the reconstruction of CDM and neutrino velocity fields from density fields [11].

CUBEP^{3}M has the added capability, vital to this work, of including neutrinos as distinct particles in the simulation. The overhead required to include neutrinos is reduced by only evolving neutrinos alongside CDM from redshift $z = 10$ and onwards. In addition, Poisson noise in the equal-time power spectra is reduced by randomly dividing each species into two groups, for which the density or velocity fields, f_1 and f_2, are calculated. The power spectrum is then computed as:

$$P(k,t) = < f_1(\mathbf{k},t) f_2(\mathbf{k},t) > \ . \tag{28}$$

Since we expect the noise in these two fields to be uncorrelated, little noise should remain in the power spectrum. Note that by the same argument, we expect there to be no noise in the unequal-time power spectra. See [11] for a more detailed explanation of the treatment of neutrinos in CUBEP^{3}M.

Initial conditions for the simulation were generated for CDM at $z = 100$ and for neutrinos at $z = 10$ using the Code for Anisotropies in the Microwave Background (CAMB) ([32], [33]). The cosmological parameters used to generate the initial conditions, chosen to be in agreement with the Planck 2015 results [15], are tabulated in Table I. We perform two simulations with almost identical initial conditions: One pure ΛCDM simulation, to calculate the gravitational potential used in the fluid equations; and one simulation with both CDM and neutrinos, to serve as a comparison to our semi-linear analysis. In the simulation of CDM and neutrinos, we include one massive neutrino species with a mass of 0.2 eV, corresponding to a cosmology with $\sum m_\nu = 0.2$ eV. Note that we can relate the physical neutrino density to the neutrino mass by [34]:

$$\Omega_\nu h^2 = \frac{\sum m_\nu}{93.14\text{eV}} \ . \tag{29}$$

A neutrino mass of 0.2 eV lies within the experimental constraints described in Section I but is large enough to allow for N-body simulations of a reasonable computational size. It is for this reason that we choose to compare our results to numerical simulations for $\sum m_\nu = 0.2$ eV. However, because the semi-analytical method used here approximates the neutrinos as linear, we expect our method to be most accurate at lower neutrino masses.

See Table II for an overview of the computational parameters chosen for these simulations. Both simulations contained 1.7×10^8 CDM particles, and the simulation with neutrinos contained 3.4×10^8 neutrino particles, twice as many as CDM. The particles were simulated in a periodic box with side length 1000 Mpc h^{-1} and gravitational forces were softened below the scale 8.3 Mpc h^{-1}. CDM particles were simulated from $z = 100$ and, in the simulation including neutrinos, neutrinos were added at $z = 10$.

B. Unequal-time correlation coefficients

We want to ensure that we retain sufficient information from the numerical simulation to compute the driving gravitational potential in the fluid equations. In the study of the effects of cosmic strings and other global defects on matter power spectra, the unequal-time correlator of the defect stress-energy tensor preserves all of the information required to compute power spectra [35, 36].

---

[38] This corresponds to $\sum m_\nu = 0.2$ eV.

Table I: The initial conditions adopted in the N-body simulations. The cosmological parameters were chosen to be in fair agreement with the Planck 2015 data [15].

Parameter	Description	Value
H_0	Hubble constant	67.0 km s^{-1} Mpc^{-1}
$\Omega_b h^2$	Physical baryon density	0.0226
$\Omega_c h^2$	Physical CDM density	0.112
Ω_k	Curvature fraction	0.0
Ω_Λ	Dark energy fraction	0.675206
T_γ	Temperature of the CMB	2.7255 K
Y	Helium mass fraction	0.24
n_s	Primordial spectral index at $k_s = 0.05$ Mpc^{-1}	0.96
A_s	Scalar amplitude	2.1×10^{-9}
σ_8	Fluctuation amplitude at 8 Mpc h^1	0.83
Ω_ν	Neutrino density	0.0048 [a]
N_{eff}	Effective number of neutrino species	3.046

Table II: Computational parameters for the CUBEP^{3}M simulations.

Parameter	Value
Number of nodes	2^3
Number of tiles per node	4^3
Box size	1000 Mpc h^{-1}
Smoothing length	8.3 Mpc h^{-1}
Number of CDM particles	1.7 $\times 10^8$
Number of neutrino particles	3.4 $\times 10^8$
Initial redshift for CDM	100
Initial redshift for neutrinos	10

As we are interested in the CDM density perturbations, we will adapt this approach by calculating the density power unequal-time correlators as a measure of the gravitational potential sourced by the perturbations. In practice, this means storing the CDM density fields over a range of redshifts. From the density fields, we can then calculate the unequal-time CDM power:

$$P_c(k,t,t') =< \delta_c(\mathbf{k},t)\delta_c^*(\mathbf{k},t') > , \tag{30}$$

where k is the magnitude of the wavevector, and the unequal-time power is found by averaging over all directions for a given magnitude k. From the unequal-time power, we construct the cross-correlation coefficient:

$$C(k,t,t') = \frac{P_c(k,t,t')}{\sqrt{P_c(k,t,t)P_c(k,t',t')}} . \tag{31}$$

It not feasible computationally to store the density fields at all time steps, and we are forced to choose times at which to calculate the cross-correlation coefficient, thereby constructing a discrete cross-correlation matrix. We will explicitly show this discrete nature by writing:

$$C_{ij}(k) \equiv C(k,t_i,t_j) . \tag{32}$$

We can eigendecompose the unequal-time matrix at a given wavenumber k:

$$C_{ij}(k) = \sum_{m=0}^{N-1} v_i^m(k)\lambda^m(k)v_j^m(k) , \tag{33}$$

where v^m are the eigenvectors, λ^m is the eigenvalue corresponding to v^m, and N is the number of redshifts at which we have recorded the density fields and therefore the size of the matrix $C_{ij}(k)$. The label m runs from 0 to $N-1$ and orders the eigenvalues in descending order, so that $m = 0$ corresponds to the principal eigenvalue and eigenvector. We now write the unequal-time CDM density power in terms of the eigenvectors and eigenvalues of the cross-correlation matrix:

$$P_{ij}(k) = \sum_{m=0}^{N-1} v_i^m(k)\sqrt{P_{ii}(k)}\lambda^m(k)\sqrt{P_{jj}(k)}v_j^m(k) . \tag{34}$$

If we define a second set of vectors, w, as:

$$w_i^m(k) = v_i^m(k)\sqrt{P_{ii}(k)}\sqrt{\lambda^m(k)} , \tag{35}$$

we may write the unequal-time power as:

$$P_{ij}(k) = \sum_{m=0}^{N-1} w_i^m(k)w_j^m(k) . \tag{36}$$

It is for this convenience of notation that we use the w-vectors throughout this work.

Note that by calculating the cross-correlation matrix, as opposed to calculating only the equal-time power spectra, we retain information on phase differences between the density fields at different redshifts. Throughout this work, we will compare our results to those obtained when this phase information is neglected and we approximate:

$$\begin{aligned} &< \delta_c(\mathbf{k},t)\delta_c(\mathbf{k},t') > \\ &\quad = \sqrt{< \delta_c(\mathbf{k},t)\delta_c(\mathbf{k},t) >< \delta_c(\mathbf{k},t')\delta_c(\mathbf{k},t') >} , \end{aligned} \tag{37}$$

consistent with the assumption made by [14]. In this approximation, all of the information on the gravitational potential is contained in the first eigenvector as only the first eigenvalue is non-zero, so that we may write:

$$w^m(k,t) = \begin{cases} \sqrt{P_c(k,t)}, & \text{if } m = 0 \ , \\ 0, & \text{otherwise} \ . \end{cases} \tag{38}$$

If the phase of the potential changes over time, we expect multiple non-zero eigenvalues in the decomposition, and therefore multiple non-zero w-vectors.

Before we proceed, we must consider what information is not included in the cross-correlation matrix. If we knew the density fields at all redshifts, and therefore were able to obtain the cross-correlation coefficients as a continuous function of t and t', the density fields at all redshifts could be reconstructed from the matrix (and the initial density field). In essence, the decomposition of the cross-correlation matrix would yield an infinite number of modes. When we choose to exclude some of these modes from the analysis (by only calculating the cross-correlation coefficients from select density fields), we are no longer able to reconstruct the density fields exactly.

To check that we have recorded an appropriate number of density fields, we examine how quickly the cross-correlation coefficients change as we move away from $t_i = t_j$. We expect that we have retained sufficient information when the cross-correlation coefficients change by less than 50% as we move two cells off-diagonal in the cross-correlation matrix. Since there is a cross-correlation matrix for each wavenumber, k, whether or not we have used enough density fields depends on the wavenumbers we are interested in. At low k, when CDM is linear, the phase changes very slowly and we do not need a large cross-correlation matrix for accurate reconstructions. However, at higher k, when the densities become non-linear, we expect the phase to change more rapidly.

IV. SIMULATION RESULTS

As discussed in Section III A, two N-body simulations were run: one with and one without massive neutrinos. In this section, the results from the simulations are presented and compared to the CLASS results with and without scaling by HALOFIT. We use the recently revised HALOFIT model [37] extended to include the effects of massive neutrinos [10]. As we are interested in the CDM and neutrino power spectra, not the matter power spectrum, throughout this report we will refer to the CLASS results scaled by the ratio of the non-linear HALOFIT and linear CLASS matter power spectra as the HALOFIT results. In Figure 1, we show the dimensionless CDM and neutrino power spectra, where the dimensionless power spectrum is defined as usual:

$$\Delta(k,t) = P(k,t)\frac{k^3}{2\pi^2} \ . \tag{39}$$

From Figure 1a we see that the CDM power spectrum agrees with linear theory at $z = 10$. At $z = 0$ however, we see that non-linearities are important for $k \gtrsim 0.1$ h Mpc^{-1}. The CDM power spectra from the simulations with and without neutrinos are consistent with one another and with the HALOFIT power spectrum at $z = 0$; this indicates that the effect of massive neutrinos on the CDM power spectrum is negligible for the neutrino masses considered in the simulation $\left(\sum m_\nu = 0.2 \text{ eV}\right)$ at $k \leq 1$ h Mpc^{-1}. The numerical neutrino power spectrum deviates strongly from linear theory at wavenumbers $k \gtrsim 0.1$ h Mpc^{-1} and as early as $z = 3$, as shown in Figure 1b. These results are consistent with previous numerical studies of the cosmic neutrino background [11, 13] and cannot be accounted for by simply scaling the linear result using HALOFIT.

In Figure 2, we show the velocity divergence power spectrum with the same normalization as the dimensionless density power spectrum:

$$\Delta_\Theta(k,t) = < \Theta(\mathbf{k},t)\Theta(\mathbf{k},t) > \frac{k^3}{2\pi^2} \ , \tag{40}$$

where $\Theta(\mathbf{k},t) = \nabla \cdot \mathbf{v}(\mathbf{k},t)$. From Figure 2a we first notice that the numerical simulations are unable to resolve the CDM velocity power spectra at $k > 0.1$ h Mpc^{-1}, possibly due to an over-subtraction of noise in the calculation. As only the CDM density fields are necessary for the semi-linear method, this is not a huge cause for concern; however, we plan to repeat this work with an improved N-body simulation in the near future. For comparison purposes only, we extend the numerical results using a second simulation with a box length of 75 Mpc h^{-1} and a softening length of 0.625 Mpc h^{-1}. As Figure 2a shows, at $z = 7$, the numerical CDM velocity divergence power agrees with linear theory, but at $z = 0$ the CDM velocity divergence power is suppressed compared to linear theory on scales $k \gtrsim 0.1$ h Mpc^{-1}, a result also noted by [11]. From Figure 2b, we see that the neutrino velocity divergence spectrum deviates from linear theory for scales $k \gtrsim 0.1$ h Mpc^{-1} at $z = 0$ but is fairly well-characterized by HALOFIT. This was also noted by [11], who find an $\approx 17\%$ error between the two spectra at $k = 1$ h Mpc^{-1}.

In Figure 3, we show the cross-correlation matrix at $k = 0.1$ h Mpc^{-1} and $k = 1.0$ h Mpc^{-1}. The cross-correlation coefficients were calculated among density fields at twelve different redshifts between $z = 0$ and $z = 15$. We see that at $k = 0.1$ h Mpc^{-1}, the cross-correlators vary slowly, indicating that the phase of the gravitational potential remains roughly constant over time; this is expected since this scale remains linear today. At $k = 1.0$ h Mpc^{-1}, the cross-correlation coefficients vary much more quickly and are close to zero for the largest redshift separations. The cross-correlation coefficient between $z = 0$ and $z = 0.5$, a term two rows off-axis in the cross-correlation matrix, is 0.4 at $k = 1.0$ h Mpc^{-1}, indicating that we expect the semi-linear method to be accurate for $k \lesssim 1.0$ h Mpc^{-1}. Because the numer-

ical simulations in this work are not accurate on scales smaller than this we choose not to collect the density field at additional redshifts in an attempt to push the accuracy to smaller scales. However, this will be necessary to test the semi-linear method on more non-linear scales, something we hope to accomplish in the near future and with higher resolution numerical simulations.

V. DENSITY POWER

In the first of three parts of this analysis, we obtain the CDM and neutrino density power spectra from the Euler equation (25) and the continuity equation (26), derived in Section II C, using the w-vectors from the numerical simulation to measure the gravitational potential as described in Section III. We therefore require a relation between the density power and the w-vectors. We start by taking the gradient of the Euler equation (25) and differentiating the continuity equation (26) with respect to time, t. Combining these equations, we obtain a single equation for the density contrast in Fourier space:

$$\frac{1}{a^2(t)}\frac{d}{dt}\left(a^2(t)\frac{d}{dt}\delta_i(\mathbf{k},t)\right) - \frac{\nabla^2 P_i}{a^2(t)\overline{\rho_i}(t)} = \frac{1}{a^2(t)}\frac{3}{2}H^2(t)a^2(t)\delta_c(\mathbf{k},t)\ . \quad (41)$$

We change the coordinate t to τ such that $\frac{d}{d\tau} = a^2\frac{d}{dt}$, $H(\tau) = a^2 H(t)$, and Equation (41) becomes:

$$\frac{d^2}{d\tau^2}\delta_i(\mathbf{k},\tau) - \frac{a^2}{\overline{\rho_i}}\nabla^2 P_i = \frac{3}{2}H^2(\tau)\delta_c(\mathbf{k},\tau)\ . \quad (42)$$

For further analysis, we must distinguish between CDM and neutrinos, as they are characterized by different pressures in the fluid approximation. As discussed above, CDM can be approximated as a pressureless fluid, while a finite pressure is necessary to account for the significant thermal motion of neutrinos. We will analyze these two cases in Sections V A and V B below.

A. Cold dark matter

We will treat CDM as a pressureless fluid with $\nabla P_c = 0$ so that Equation (42) can be written as:

$$\ddot{\delta}_c(\mathbf{k},\tau) = \frac{3}{2}H^2(\tau)\delta_c(\mathbf{k},\tau)\ , \quad (43)$$

where $\dot{f}$ now indicates the derivative of f with respect to τ and $H(\tau) = \frac{\dot{a}}{a}$. A Green's function solution to Equation (43) with $G_c(\tau,\tau') = \tau - \tau'$ exists:

$$\delta_c(\mathbf{k},\tau) = \int_{-\infty}^{\tau} d\tau'(\tau-\tau')\frac{3}{2}H^2(\tau)\delta_c(\mathbf{k},\tau')\ , \quad (44)$$

so that we may write the density power:

$$P_c(\tau) = <\delta_c(\tau)\delta_c^*(\tau)> = \int_{-\infty}^{\tau} d\tau'(\tau-\tau')\frac{3}{2}H^2(\tau')\int_{-\infty}^{\tau} d\tau''(\tau-\tau'')\frac{3}{2}H^2(\tau'') <\delta_c(\tau')\delta_c^*(\tau'')>\ . \quad (45)$$

For convenience of notation, we will not explicitly indicate the dependence of the power spectra, w-vectors, and density fields on $\mathbf{k}$ although it is implied. Using Equation (36) for the unequal-time CDM power, we can rewrite Equation (45) as:

$$P_c(\tau) = \sum_m \left|\int_{-\infty}^{\tau} d\tau'(\tau-\tau')\frac{3}{2}H^2(\tau')w^m(\tau')\right|^2\ . \quad (46)$$

Therefore, by performing integrals over the w-vectors, we can reconstruct the CDM density power.

B. Massive neutrinos

As mentioned in Section II B, neutrinos may be treated as a fluid with a finite sound speed $c_s^2 = \frac{\overline{c_s}^{-2}}{a^2}$. Recall that the sound speed is related to the pressure gradient via:

$$c_s^2 = \frac{\partial P}{\partial \rho} = \frac{\nabla P}{\nabla \rho} = \frac{\nabla P}{\bar{\rho}\nabla\delta}\ , \quad (47)$$

so that we may rewrite Equation (42) as:

$$\ddot{\delta_\nu}(\mathbf{k},\tau) + k^2\overline{c_s}^2\delta_\nu(\mathbf{k},\tau) = \frac{3}{2}H^2(\tau)\delta_c(\mathbf{k},\tau)\ . \quad (48)$$

We now change coordinates to a new time τ such that $\frac{d}{d\tau} = \frac{a^2}{k\overline{c_s}}\frac{d}{dt}$. In these coordinates, Equation (48) reduces to:

$$\ddot{\delta_\nu} + \delta_\nu = \frac{3}{2}H^2(\tau)\delta_c\ , \quad (49)$$

where $\dot{f}$ now indicates a derivative of f with respect to the new variable τ and $H(\tau) = \frac{\dot{a}}{a}$. A Green's function solution to Equation (49) with $G_\nu(\tau,\tau') = \sin(\tau-\tau')$ exists:

$$\delta_\nu(\mathbf{k},\tau) = \int_{-\infty}^{\tau} d\tau'\sin(\tau-\tau')\frac{3}{2}H^2(\tau')\delta_c(\mathbf{k},\tau')\ . \quad (50)$$

As we did for CDM in Section V A, we can obtain an equation for the neutrino density power in terms of the w-vectors. We start with:

$$P_\nu(\tau) = <\delta_\nu(\tau)\delta_\nu^*(\tau)> = \int_{-\infty}^{\tau} d\tau'\sin(\tau-\tau')\frac{3}{2}H^2(\tau')\int_{-\infty}^{\tau} d\tau''\sin(\tau-\tau'')\frac{3}{2}H^2(\tau'') <\delta_c(\tau')\delta_c^*(\tau'')>\ , \quad (51)$$

where once again the dependence of the power, density and w-vectors on $\mathbf{k}$ is implied. Using Equation (36) we can write:

$$P_\nu(\tau) = \sum_m \left| \int_{-\infty}^{\tau} d\tau' \sin(\tau - \tau') \frac{3}{2} H^2(\tau') w^m(\tau') \right|^2 . \tag{52}$$

Therefore, we can calculate the neutrino power spectrum in the same manner as the CDM power spectrum, but with a slightly different Green's function.

C. The matter dominated regime

Since the numerical data spans a finite redshift range, we must find analytic expressions for the integrals in Equations (46) and (52) at high redshifts. We use the numerical potential at redshifts $z = 15$ and lower, as at these redshifts there are no artifacts of the initial particle grid in the N-body power spectra. It is justified to assume matter domination when calculating the early time integrals since at $z = 15$ the universe is matter dominated $\left(\frac{\Omega_M a^3}{\Omega_\Lambda} \approx 1500 \right)$. Under this assumption, the CDM density contrast scales linearly with the scalefactor. We assume that the phase of the gravitational potential remains constant at these early times, so that we may take the unequal-time CDM power spectrum to be:

$$P_{c,M}(k, \tau, \tau') = A^2(k) a(\tau) a(\tau') , \tag{53}$$

where $A(k)$ is determined by normalizing the power spectrum to the numerical results at $z = 15$ and we have used the subscript M to indicate quantities in matter domination. Note that we normalize at $z = 15$ instead of $z = 0$ in order to reduce the propagation of non-linear effects to high redshifts. This gives the w-vectors:

$$w_M^m(k, \tau) = \begin{cases} A(k) a(\tau), & \text{if } m = 0 , \\ 0, & \text{otherwise} , \end{cases} \tag{54}$$

and we will use the Hubble parameter in matter domination:

$$H_M(t) = H_0 \sqrt{\frac{\Omega_M}{a^3(t)}} . \tag{55}$$

Using Equations (54) and (55) we will derive analytical expressions for Equations (46) and (52), the semi-linear CDM and neutrino power spectra respectively, in Sections V C 1 and V C 2 below.

1. Cold dark matter

For CDM, the time τ is related to the proper time t by:

$$\frac{dt}{d\tau} = a^2 , \tag{56}$$

so that we can write:

$$\begin{aligned} H_M(\tau) &= \frac{1}{a} \frac{dt}{d\tau} \frac{da}{dt} \\ &= a^2(\tau) H_0 \sqrt{\frac{\Omega_M}{a^3(\tau)}} . \end{aligned} \tag{57}$$

This gives the following relationship between τ and the scalefactor, a:

$$\tau = \frac{-2}{H_0 \sqrt{\Omega_M}} \frac{1}{a^{1/2}} . \tag{58}$$

Using these relations, we find that the integral over early times is:

$$\begin{aligned} I_{c,M}(k, \tau, \tau_0) &= \int_{-\infty}^{\tau_0} d\tau' (\tau - \tau') \frac{3}{2} H^2(\tau') A(k) a(\tau') \\ &= \frac{24 A(k)}{H_0^2 \Omega_M} \left(\frac{1}{2\tau_0^2} - \frac{\tau}{3\tau_0^2} \right) , \end{aligned} \tag{59}$$

where τ is the time at which the power is being calculated and τ_0 is the earliest time at which we use the numerical potential in the integration. The subscript M indicates that the integral is calculated under the assumption of matter domination. In order to calculate the fully analytic result, we simply set $\tau_0 = \tau$:

$$\begin{aligned} P_{c,M}(k, \tau) &= \left| \int_{-\infty}^{\tau} d\tau' (\tau - \tau') \frac{3}{2} H^2(\tau') A(k) a(\tau') \right|^2 \\ &= A^2(k) a^2(\tau) . \end{aligned} \tag{60}$$

Therefore, Equation (59) reduces to the correct expression for the CDM power spectrum in matter domination.

2. Massive neutrinos

For neutrinos, the method is similar. For the time coordinate τ in Equation (52), we find:

$$\begin{aligned} H_M(\tau) &= \frac{1}{a} \frac{d}{d\tau} \frac{da}{dt} \\ &= \frac{a^2(\tau)}{k \overline{c_s}} H_0 \sqrt{\frac{\Omega_m}{a^3(\tau)}} \end{aligned} \tag{61}$$

and

$$\tau = \frac{-2 k \overline{c_s}}{H_0 \sqrt{\Omega_M}} \frac{1}{a^{1/2}} . \tag{62}$$

Therefore, the integral over early times is:

$$\begin{aligned} I_{\nu,M}(k, \tau, \tau_0) = &\int_{-\infty}^{\tau_0} d\tau' \sin(\tau - \tau') \frac{3}{2} H^2(\tau') A(k) a(\tau') \\ = &\frac{24 k^2 \overline{c_s}^2}{H_0^2 \Omega_M} A(k) \frac{1}{12\tau_0^3} (2\tau_0 \cos(\tau - \tau_0) + \\ &2\tau_0^3 \cos(\tau) \mathrm{Ci}(-\tau_0) + \\ &\pi \tau_0^3 \sin(\tau) + 2\left(-2 + \tau_0^2\right) \sin(\tau - \tau_0) + \\ &2\tau_0^3 \sin(\tau) \mathrm{Si}(\tau_0)) , \end{aligned} \tag{63}$$

where Si and Ci are the sine integral and cosine integral functions,

$$\mathrm{Si}(x) = \int_0^x \frac{\sin(y)}{y} dy \tag{64}$$

and

$$\mathrm{Ci}(x) = -\int_x^\infty \frac{\cos(y)}{y} dy \tag{65}$$

respectively. Once again, we can obtain a purely analytic expression for the neutrino power spectrum in the matter dominated regime by setting $\tau_0 = \tau$. In this case, the expression above reduces to:

$$\begin{aligned} P_{\nu,M}(k,\tau) =& \left| \int_{-\infty}^{\tau} d\tau' \sin(\tau-\tau') \frac{3}{2} H^2 \tau' A(k) a(\tau') \right|^2 \\ =& \left| \frac{24 k^2 \overline{c_s}^2 A(k)}{H_0^2 \Omega_M} \frac{1}{12} \Big(\frac{2}{\tau^2} + \right. \\ & \left. 2\cos(\tau)\mathrm{CI}(-\tau) + \sin(\tau)\big(\pi + 2\mathrm{SI}(\tau)\big) \Big) \right|^2 . \end{aligned} \tag{66}$$

D. Density power results

We now have all of the information required to calculate the CDM and neutrino density powers. We will break down Equations (46) and (52) as follows:

$$\begin{aligned} P_i(k,\tau) =& \left| I_{i,M}(k,\tau,\tau_0) + \right. \\ & \left. \int_{\tau_0}^{\tau} d\tau' G_i(\tau-\tau') \frac{3}{2} H^2(\tau') w^0(k,\tau') \right|^2 + \\ & \sum_{m=1}^{m_{max}} \left| \int_{\tau_0}^{\tau} d\tau' G_i(\tau-\tau') \frac{3}{2} H^2(\tau') w^m(k,\tau') \right|^2 , \end{aligned} \tag{67}$$

where we use the analytic integrals $I_{i,M}$ from Equations (59) and (**??**). The remaining integrals were calculated numerically using a trapezoidal integration method after interpolating the w-vectors over redshift.

In Figure 4 we compare the semi-linear CDM power spectrum at redshift $z = 0$ to the CLASS, HALOFIT, and numerical power spectra. We find that the semi-linear method does not improve significantly on linear theory. This is not surprising, as a linear treatment of CDM is expected to break down on small scales and at late times when CDM clusters significantly. We also note that the semi-linear power is highest when phase changes in the gravitational potential are ignored. This follows from the Cauchy-Schwarz inequality, which states that the cross-power between two fields is largest when they are in phase.

In Figure 5, we show the semi-linear neutrino power spectrum for both $\sum m_\nu = 0.2$ eV (Figure 5a) and $\sum m_\nu = 0.1$ eV (Figure 5b). In contrast to the CDM results, the semi-linear neutrino power spectra are an improvement on both linear theory and HALOFIT and agree with the numerical power spectrum for $k \lesssim 0.2$ h Mpc^{-1}, even when only the primary w-vector is included in the calculation. We find that increasing the number of w-vectors included causes the small scale power to increase, improving the error at small scales; however it does not increase the range of wavenumbers at which this method provides an accurate representation of the N-body power spectrum. We also see that when we include many modes the results agree well with those obtained when the phase of the gravitational potential is assumed to be unchanging.

VI. VELOCITY POWER

The method described in this report can be used to calculate many fluid properties via the fluid equations. In this section, we discuss using this method to obtain the velocity divergence power spectrum. From the continuity equation (26), we can write the velocity divergence, $\Theta_i(\mathbf{k},t)$, in terms of the density perturbation:

$$\Theta_i(\mathbf{k},t) = \nabla \cdot \mathbf{u}_i(\mathbf{k},t) = -a \frac{\partial \delta_i(\mathbf{k},t)}{\partial t} = -a \frac{\partial \tau}{\partial t} \frac{\partial \delta_i(\mathbf{k},t)}{\partial \tau} . \tag{68}$$

Therefore by using Equations (44) and (50) for the CDM and neutrino density perturbations, we can calculate the velocity divergence power for both species. In Fourier space, the velocity and the velocity divergence are closely related by $\nabla \cdot \mathbf{u} = i\mathbf{k} \cdot \mathbf{u}$. Therefore, we can calculate the power of the velocity magnitude from the velocity divergence power. The calculation of the velocity divergence power is described in more detail for both CDM and neutrinos in Sections VI A and VI B.

A. Cold dark matter

Using Equation (44) for the CDM density perturbation, we can expand Equation (68) as follows:

$$\begin{aligned} \Theta_c(\mathbf{k},\tau) &= \nabla \cdot \mathbf{u}_c(\mathbf{k},\tau) \\ &= -a(\tau) \frac{\partial \tau}{\partial t} \frac{\partial \delta_c(\mathbf{k},\tau)}{\partial \tau} \\ &= -\frac{1}{a(\tau)} \frac{d}{d\tau} \int_{-\infty}^{\tau} d\tau' (\tau-\tau') \frac{3}{2} H^2(\tau') \delta_c(\mathbf{k},\tau') \\ &= -\frac{1}{a(\tau)} \int_{-\infty}^{\tau} d\tau' \frac{3}{2} H^2(\tau') \delta_c(\mathbf{k},\tau') . \end{aligned} \tag{69}$$

We write the velocity divergence power in terms of the w-vectors as we did for the density power:

$$\begin{aligned}P_{\Theta_c}(k,\tau) =& < \Theta_c(\mathbf{k},\tau)\Theta_c^*(\mathbf{k},\tau) > \\ =&\frac{1}{a^2(\tau)}\int_{-\infty}^{\tau} d\tau' \frac{3}{2}H^2(\tau') \\ &\int_{-\infty}^{\tau} d\tau'' \frac{3}{2}H^2(\tau'') < \delta_c(\mathbf{k},\tau')\delta_c^*(\mathbf{k},\tau'') > \\ =&\frac{1}{a^2(\tau)}\sum_m \left| \int_{-\infty}^{\tau} d\tau' \frac{3}{2}H^2(\tau') w^m(k,\tau') \right|^2 .\end{aligned} \tag{70}$$

Note that integral in Equation (70) is essentially a Green's function integral with a Green's function $G_{\Theta_c}(\tau,\tau') = 1$.

We need expressions for evaluating the integral in Equation (70) at early times, when we do not have numerical data from the simulation. As in Section V, we will calculate this integral at early times under the assumption of matter domination using Equations (54) and (55) for the w-vectors and Hubble factor respectively, resulting in:

$$\begin{aligned}I_{\Theta_c,M}(k,\tau,\tau_0) =& \int_{-\infty}^{\tau_0} d\tau' \frac{3}{2}a(\tau')^4 H_0^2 \Omega_M A(k) a(\tau') \\ =& \frac{-1}{3}\frac{24A(k)}{H_0^2\Omega_M}\frac{1}{\tau_0^3} .\end{aligned} \tag{71}$$

To obtain a purely analytic expression for the CDM velocity divergence power in the matter dominated era, we set $\tau_0 = \tau$ in Equation (71):

$$I_{\Theta_c,M}(k,\tau,\tau) = -\frac{8A(k)}{H_0^2\Omega_M}\frac{1}{\tau^3} . \tag{72}$$

Substituting this into the Equation (70) we obtain:

$$P_{\Theta_c,M}(k,\tau) = \frac{1}{a^2(\tau)}\left|\frac{8A(k)}{H_0^2\Omega_M}\frac{1}{\tau^3}\right|^2 . \tag{73}$$

B. Massive neutrinos

Along the same lines as in Section VI A, we can expand Equation (68) using Equation (50) for the neutrino density perturbation as follows:

$$\begin{aligned}\Theta_\nu(\mathbf{k},\tau) =& \nabla\cdot\mathbf{u}_\nu(\mathbf{k},\tau) \\ =& -a(\tau)\frac{\partial\tau}{\partial t}\frac{\partial\delta_c(\mathbf{k},\tau)}{\partial\tau} \\ =& -\frac{k\overline{c_s}}{a(\tau)}\frac{d}{d\tau}\int_{-\infty}^{\tau} d\tau' \sin(\tau-\tau')\frac{3}{2}H^2(\tau')\delta_c(\mathbf{k},\tau') \\ =& -\frac{k\overline{c_s}}{a(\tau)}\int_{-\infty}^{\tau} d\tau' \cos(\tau-\tau')\frac{3}{2}H^2(\tau')\delta_c(\mathbf{k},\tau') .\end{aligned} \tag{74}$$

We can now express the neutrino velocity divergence power in terms of the w-vectors:

$$\begin{aligned}P_{\Theta_\nu}(k,\tau) =& < \Theta_\nu(\mathbf{k},\tau)\Theta_\nu^*(\mathbf{k},\tau) > \\ =&\left(\frac{k\overline{c_s}}{a(\tau)}\right)^2\int_{-\infty}^{\tau} d\tau' \cos(\tau-\tau')\frac{3}{2}H^2(\tau') \\ &\int_{-\infty}^{\tau} d\tau'' \cos(\tau-\tau'')\frac{3}{2}H^2(\tau'') < \delta_c(\mathbf{k},\tau')\delta_c^*(\mathbf{k},\tau'') > \\ =&\left(\frac{k\overline{c_s}}{a(\tau)}\right)^2\sum_m \left| \int_{-\infty}^{\tau} d\tau' \cos(\tau-\tau') \right. \\ &\left. \frac{3}{2}H^2(\tau') w^m(k,\tau') \right|^2 .\end{aligned} \tag{75}$$

This is analogous to a Green's function solution with $G_{\Theta_\nu}(\tau,\tau') = \cos(\tau-\tau')$.

Once again, we require expressions for the relevant integrals at early times, when we lack numerical data. Under the assumption of matter domination, using equations (54) and (55) for the w-vectors and the Hubble factor, we obtain:

$$\begin{aligned}I_{\Theta_\nu,M}(k,\tau,\tau_0) =& \int_{-\infty}^{\tau_0} d\tau' \cos(\tau-\tau')\frac{3}{2}\frac{a^4(\tau')}{k^2\overline{c_s}^2}H_0^2\frac{\Omega_M}{a^3(\tau')}A(k)a(\tau') \\ =&\frac{24k^2\overline{c_s}^2A(k)}{H_0^2\Omega_M}\frac{1}{12\tau_0^3}\Big(\pi\tau_0^3\cos(\tau)+ \\ &2(\tau_0^2-2)\cos(\tau-\tau_0)- \\ &2\tau_0(\sin(\tau-\tau_0)+\tau_0^2(\mathrm{CI}(-\tau_0)\sin(\tau)- \\ &\cos(\tau)\mathrm{SI}(\tau_0)))\Big)\end{aligned} \tag{76}$$

We can find an analytic expression for the neutrino velocity divergence power by setting $\tau_0 = \tau$ in the above expression:

$$\begin{aligned}I_{\Theta_\nu,M}(k,\tau,\tau) =&\frac{24k^2\overline{c_s}^2A(k)}{H_0^2\Omega_M}\frac{1}{12}\Big(\frac{2(\tau^2-2)}{\tau^3}- \\ &2\mathrm{CI}(-\tau)\sin(\tau)+\cos(\tau)(\pi+2\mathrm{SI}(\tau))\Big) .\end{aligned} \tag{77}$$

Substituting this into Equation (75) we find an expression for the neutrino velocity divergence power in matter domination:

$$\begin{aligned}P_{\Theta_\nu,M}(k,\tau) =&\left(\frac{k\overline{c_s}}{a(\tau)}\right)^2\left|\frac{24k^2\overline{c_s}^2A(k)}{H_0^2\Omega_M}\frac{1}{12}\Big(\pi\tau_0^3\cos(\tau)+\right. \\ &2(\tau_0^2-2)\cos(\tau-\tau_0)-2\tau_0(\sin(\tau-\tau_0)+ \\ &\left.\tau_0^2(\mathrm{CI}(-\tau_0)\sin(\tau)-\cos(\tau)\mathrm{SI}(\tau_0)))\Big)\right|^2 .\end{aligned} \tag{78}$$

C. Velocity divergence results

Analogous to our treatment of the density power, to calculate the CDM or neutrino velocity divergence power

using Equation (70) or (75) respectively, we decompose the relevant integral as follows:

$$P_{\Theta_i}(k,\tau) = \Big| I_{\Theta_i,M}(k,\tau,\tau_0) + \int_{\tau_0}^{\tau} d\tau' G_{\Theta_i}(\tau-\tau')\frac{3}{2}H^2(\tau')w^0(k,\tau')\Big|^2 + \sum_{m=1}^{m_{max}} \Big| \int_{\tau_0}^{\tau} d\tau' G_{\Theta_i}(\tau-\tau')\frac{3}{2}H^2(\tau')w^m(k,\tau')\Big|^2 . \quad (79)$$

Figure 6 shows the CDM velocity divergence power spectra from CLASS, the simulation, and the semi-linear method. The results are similar to those for the CDM density power. Again, we see that the semi-linear method does not improve significantly on the linear results, and that the semi-linear results obtained with twelve eigenmodes agree well with those obtained when the phase of the gravitational potential is ignored. Interestingly, we see that even though the N-body CDM velocity divergence spectrum is reduced from linear theory on small scales, adding additional modes to the semi-linear calculation increases the power on small scales, suggesting that including the non-linear gravitational potential and accounting for the phase of the gravitational potential do not to explain this departure from linearity.

In Figure 7, the neutrino velocity divergence power is shown for $\sum m_\nu = 0.2$ eV (Figure 7a) and $\sum m_\nu = 0.1$ eV (Figure 7b). Here, we see that the semi-linear results are a significant correction to linear theory and agree well with both the numerical and HALOFIT power spectra. Again, we note that when all modes are included, the results agree with those obtained when changes in the gravitational potential phase are ignored.

VII. INCLUDING NON-LINEARITIES IN THE FLUID EQUATIONS

A possible improvement to this semi-linear approach is the inclusion of non-linear terms in the fluid equations. While this seems a natural direction to pursue, non-linear terms containing both δ_ν and δ_c complicate the integration of the fluid equations to calculate neutrino perturbations. However, considering that neutrino density perturbations are much smaller than CDM density perturbations, it is possible to include these non-linear terms through an iterative approach. In this section, we investigate this technique; however, we leave a rigorous treatment of the non-linearities to future work.

If we repeat the derivation of the comoving fluid equations in Section II but do not linearize the fluid equations, we can consider the effects of higher order perturbations to the CDM and neutrino density and velocity fluctuations. We start with the full compressible fluid equations in the Newtonian gauge before conversion to comoving coordinates, Equations (8) and (9), reproduced here for convenience:

$$\frac{\partial \rho}{\partial t} + \nabla\cdot(\rho\mathbf{v}) = 0 \quad (80)$$

and

$$\frac{\partial \rho\mathbf{v}}{\partial t} + (\mathbf{v}\cdot\nabla)(\rho\mathbf{v}) + \nabla P_T = 0\,. \quad (81)$$

By differentiating Equation (80) with respect to t and taking the divergence of Equation (81) we obtain, after some manipulation, the single equation:

$$\frac{\partial^2\rho}{\partial t^2} - \nabla\cdot((\mathbf{v}\cdot\nabla)\rho\mathbf{v}) = \nabla^2 P - \nabla(\rho\nabla\Phi)\,, \quad (82)$$

where P is the pressure that is not due to gravity. After converting to comoving coordinates and linearizing Equation (82) with respect to the variable $\mathbf{u}$ only, we obtain the equation:

$$\ddot{\delta}_i - \frac{a^2}{\overline{\rho_i}}\nabla^2 P = a^2\nabla((1+\delta_i)\nabla(\phi_c)) = \frac{3}{2}H^2(\tau)\nabla((1+\delta_i)\nabla\phi_c)\,, \quad (83)$$

where a coordinate transformation from t to τ has been made such that $\frac{d}{d\tau} = a^2\frac{d}{dt}$, $\dot{f}$ is the derivative of f with respect to τ, and $H(\tau) = \frac{1}{a}\frac{da}{d\tau}$. Equation (82) is linearized with respect to $\mathbf{u}$ but not δ as we expect the density perturbation to be more significant than the velocity perturbation, as seen throughout this analysis (*e.g.* Figures 1 and 2).

Equation (83) differs from Equation (42), the linearized equation for the density perturbation, by only the right hand side. Therefore, to obtain the density power spectra from Equation (83), we can use the same Green's functions as in Section V. The change in the right hand side is accounted for by defining a new set of vectors, z_i, analogous to the w-vectors so that:

$$<(\nabla((1+\delta_i(\tau))\nabla\delta_c(\tau))(\nabla((1+\delta_i(\tau'))\nabla\delta_c(\tau')))^*> = \sum_m z_i^m(\tau)z_i^m(\tau')\,, \quad (84)$$

where we have suppressed the k dependence of δ and z. Note that we require a set of z-vectors for both neutrinos ($i=\nu$) and CDM ($i=c$), and that we need the neutrino density field to define z_ν. We can write the density power as:

$$P_{i,z}(k,\tau) = \sum_m \Big| \int_{-\infty}^{\tau} d\tau' G_i(\tau,\tau')\frac{3}{2}H^2(\tau')z_i^m(k,\tau')\Big|^2\,, \quad (85)$$

where the subscript z indicates that this is the power driven by the z-vectors, and $G_i(\tau,\tau')$ are the Green's functions from Section V:

$$G_c(\tau,\tau') = \tau - \tau' \quad (86)$$

and

$$G_\nu(\tau,\tau') = \sin(\tau-\tau')\,. \quad (87)$$

When calculating the CDM density power spectrum from Equation (85), we obtain the driving term $\nabla((1+\delta_c)\nabla\delta_c)$ from numerical simulations. Similarly, we can calculate the z_ν-vectors using density fields from the simulation including neutrinos. However, as our goal is to replace N-body simulations of neutrinos with a semi-linear method, we would like to omit any dependence on the neutrino density fields from simulations. This can be done by generating neutrino density fields at the desired redshifts using the initial conditions generator for CUBEP^{3}M. If we normalize the density fields to the neutrino power spectra driven by the w-vectors from Section V, they can be used to calculate the z-vectors and the neutrino response to the $\nabla((1+\delta_\nu)\nabla\phi_c)$ driving term. This process can then be repeated using the newly obtained neutrino power spectra to normalize the neutrino density fields. We can reiterate this procedure until the results converge. In the results presented below, only four iterations of this method were used.

In Figure 8, we show the density power spectra of CDM and neutrinos calculated from Equation (85). As can be seen from Figure 8b, the neutrino density power spectrum calculated at 4th order in the iterative method has a higher power than the 0th order results (*i.e.*, the results calculated from the w-vectors), but convergence towards the power calculated using the z-vectors from the numerical simulation is slow. A likely reason for the slow convergence is that the neutrino density fields are generated with random phases and therefore we expect little to no cross-correlation between the neutrino and CDM density fields on small scales in the iterative method. In contrast, when using the N-body fields, we expect a significant cross-correlation between the neutrino and CDM density fields as neutrinos are most likely to cluster where CDM is significantly clustered. A more realistic treatment of the neutrino density fields is therefore one in which we assume that the neutrino and CDM densities are in phase, so that we can write:

$$\delta_\nu(\mathbf{k},t) = \sqrt{\frac{P_\nu(k,t)}{P_c(k,t)}}\delta_c(\mathbf{k},t)\ . \tag{88}$$

We will investigate this method in future work.

Figure 8 shows that for both CDM and neutrinos, the density power response to the z-vectors is significantly larger than the N-body power spectrum even at very low k. This is likely due to terms omitted from the fluid equations, including higher order terms in the velocity perturbation. Another possibility is that the pressure experienced by CDM and neutrinos is underestimated at late times and on small scales. Indeed, in our analysis we treat CDM as a pressureless fluid; however, when CDM clusters this assumption is no longer valid; in order for halos to be in static equilibrium, the clustered CDM must be experiencing an outward pressure to balance the inward gravitational pressure. An outward pressure would resist structure formation and therefore reduce the power on small scales, driving the power spectrum in the correct direction. To investigate the effects of the pressure more thoroughly, the CDM pressure can be calculated from numerical simulations and incorporated into the fluid equations. We will pursue these possible additions to the non-linear fluid equations in future work.

VIII. CONCLUSIONS AND FUTURE WORK

We have presented a semi-linear treatment of neutrinos in a ΛCDM universe that includes the fully non-linear behaviour of CDM from N-body simulations. While this method succeeds at improving upon linear theory, it does not accurately reproduce the N-body neutrino power spectrum for $k \gtrsim 0.2$ h Mpc^{-1}. The numerical neutrino velocity divergence power, however, is well-characterized by this semi-linear method. The relative success of the application of the semi-linear method to the neutrino velocity divergence power compared to the neutrino density power may be due to the fact that the velocity divergence tends to be better characterized by linear theory than the density. Using unequal-time cross-correlation coefficients to retain phase information on the gravitational potential from the N-body simulation allows us to discuss the effects of subordinate modes on the power spectra; however, when many modes are included the results converge to those obtained when the phase of the gravitational potential is assumed to be constant with redshift. This method applied to CDM provides little improvement on linear theory, as is expected: A fluid approximation of CDM is obviously inappropriate when the CDM density field is non-linear.

The inaccuracy of this method compared to the N-body neutrino power spectrum on small scales indicates that a linear fluid treatment of neutrinos on these scales may not be appropriate. In future work, we hope to improve upon these results by including higher order perturbations in the neutrino fluid equations. To provide a more conclusive analysis of this method, we must also look at running high resolution simulations to successfully model the power spectra on smaller scales. We can match this with the semi-linear method by including more modes in our decomposition of the unequal-time cross correlation matrix, thereby testing the applicability of this method to modelling non-linearities on much smaller scales than those discussed in this work.

The semi-linear method proposed in this work allows for the study of non-linear neutrino behaviour without relying on N-body simulations of neutrinos. As a result, it is very rapid and simple to implement. Since it is easy to include various fluid properties in the analytic treatment of neutrinos, this semi-linear method is well-suited to the investigation of the effects these properties have on the neutrino power spectra. For example, very low mass neutrinos or neutrinos with a time-varying mass are extremely difficult to simulate numerically but are easily modelled using this semi-linear method. Studies of non-linear neutrino behaviour are important for predict-

ing and interpreting the results of future searches for direct detections of relic neutrinos, such as the PTOLEMY experiment. If we understand non-linear neutrino behaviour and its dependence on cosmology, studies of cosmic neutrinos stand to provide insight not only into neutrinos but also into the early universe they probe.

Acknowledgments

I would like to thank Derek Inman and J.D. Emberson for their support with the CUBEP^{3}M simulations. Computations were performed on the GPC supercomputer at the SciNet HPC Consortium. SciNet is funded by: the Canada Foundation for Innovation under the auspices of Compute Canada; the Government of Ontario; Ontario Research Fund - Research Excellence; and the University of Toronto.

[1] T. Schwetz, M. Tortola, and J. W. F. Valle, New J. Phys. **13**, 063004 (2011), 1103.0734.
[2] P. Guzowski, in *Topical Research Meeting on Prospects in Neutrino Physics (NuPhys2014) London, UK, United Kingdom, December 15-17, 2014* (2015), 1504.08285, URL `http://inspirehep.net/record/1365552/files/arXiv:1504.08285.pdf`.
[3] J. Lesgourgues and S. Pastor, Phys. Rept. **429**, 307 (2006), astro-ph/0603494.
[4] Y. Y. Y. Wong, Ann. Rev. Nucl. Part. Sci. **61**, 69 (2011), 1111.1436.
[5] P. A. R. Ade et al. (Planck) (2015), 1502.01591.
[6] S. Riemer-Sørensen, D. Parkinson, and T. M. Davis, Phys. Rev. **D89**, 103505 (2014), 1306.4153.
[7] P. Schneider, *Extragalactic Astronomy and Cosmology: An Introduction* (Springer, 2015), chap. 7, 2nd ed.
[8] S. Betts et al., in *Community Summer Study 2013: Snowmass on the Mississippi (CSS2013) Minneapolis, MN, USA, July 29-August 6, 2013* (2013), 1307.4738, URL `http://www.slac.stanford.edu/econf/C1307292/docs/submittedArxivFiles/1307.4738.pdf`.
[9] J. Brandbyge and S. Hannestad, JCAP **0905**, 002 (2009), 0812.3149.
[10] S. Bird, M. Viel, and M. G. Haehnelt, Mon. Not. Roy. Astron. Soc. **420**, 2551 (2012), 1109.4416.
[11] D. Inman, J. Emberson, U.-L. Pen, A. Farchi, H.-R. Yu, and J. Harnois-Déraps, Phys. Rev. **D92**, 023502 (2015), 1503.07480.
[12] J. Brandbyge and S. Hannestad, JCAP **1001**, 021 (2010), 0908.1969.
[13] J. Brandbyge, S. Hannestad, T. Haugbolle, and B. Thomsen, JCAP **0808**, 020 (2008), 0802.3700.
[14] Y. Ali-Haïmoud and S. Bird, Mon. Not. Roy. Astron. Soc. **428**, 3375 (2012), 1209.0461.
[15] P. A. R. Ade et al. (Planck) (2015), 1502.01589.
[16] J. Lesgourgues (2011), 1104.2932.
[17] W. H. Press and P. Schechter, Astrophys. J. **187**, 425 (1974).
[18] M. Boylan-Kolchin, V. Springel, S. D. M. White, A. Jenkins, and G. Lemson, Mon. Not. Roy. Astron. Soc. **398**, 1150 (2009), 0903.3041.
[19] J. R. Bond and A. S. Szalay, Astrophys. J. **274**, 443 (1983).
[20] J. A. Holtzman, Astrophys. J. Suppl. **71**, 1 (1989).
[21] M. Shoji and E. Komatsu, Phys. Rev. **D81**, 123516 (2010), [Erratum: Phys. Rev.D82,089901(2010)], 1003.0942.
[22] J. Lesgourgues and T. Tram, JCAP **1109**, 032 (2011), 1104.2935.
[23] P. Peebles, *Principles of Physical Cosmology* (Princeton University Press, 1993), chap. 5.
[24] D. Baumann, *Lecture notes in cosmology*, URL `http://www.damtp.cam.ac.uk/user/db275/Cosmology/Chapter4.pdf`.
[25] J. Harnois-Déraps, U.-L. Pen, I. T. Iliev, H. Merz, J. D. Emberson, and V. Desjacques, Mon. Not. Roy. Astron. Soc. **436**, 540 (2013), 1208.5098.
[26] C. Loken, D. Gruner, L. Groer, R. Peltier, N. Bunn, M. Craig, T. Henriques, J. Dempsey, C.-H. Yu, J. Chen, et al., Journal of Physics: Conference Series **256**, 012026 (2010), URL `http://stacks.iop.org/1742-6596/256/i=1/a=012026`.
[27] H. Merz, U.-L. Pen, and H. Trac, New Astron. **10**, 393 (2005), astro-ph/0402443.
[28] H. Park, P. R. Shapiro, E. Komatsu, I. T. Iliev, K. Ahn, and G. Mellema, Astrophys. J. **769**, 93 (2013), 1301.3607.
[29] H. Park, E. Komatsu, P. R. Shapiro, J. Koda, and Y. Mao (2015), 1506.05177.
[30] I. T. Iliev, G. Mellema, K. Ahn, P. R. Shapiro, Y. Mao, and U.-L. Pen, Mon. Not. Roy. Astron. Soc. **439**, 725 (2014), 1310.7463.
[31] S. Majumdar, G. Mellema, K. K. Datta, H. Jensen, T. R. Choudhury, S. Bharadwaj, and M. M. Friedrich, Mon. Not. Roy. Astron. Soc. **443**, 2843 (2014), 1403.0941.
[32] A. Lewis, A. Challinor, and A. Lasenby, Astrophys. J. **538**, 473 (2000), astro-ph/9911177.
[33] A. Lewis, Phys. Rev. **D87**, 103529 (2013), 1304.4473.
[34] G. Mangano, G. Miele, S. Pastor, T. Pinto, O. Pisanti, and P. D. Serpico, Nucl. Phys. **B729**, 221 (2005), hep-ph/0506164.
[35] U.-L. Pen, D. N. Spergel, and N. Turok, Phys. Rev. **D49**, 692 (1994).
[36] U.-L. Pen, U. Seljak, and N. Turok, Phys. Rev. Lett. **79**, 1611 (1997), astro-ph/9704165.
[37] R. Takahashi, M. Sato, T. Nishimichi, A. Taruya, and M. Oguri, Astrophys. J. **761**, 152 (2012), 1208.2701.
[38] D. Baumann, *Lecture notes in cosmology*, URL `http://www.damtp.cam.ac.uk/user/db275/Cosmology/Chapter3.pdf`.

Appendix A: Relating the Neutrino and Photon Temperatures

We can relate the cosmic neutrino background and CMB temperatures as follows. Before decoupling, neutrinos and photons were in thermal equilibrium. After decoupling, both the photon and neutrino temperatures decreased due to the expansion of the universe: $T \propto a^{-1}$. However, in addition to this decrease, the temperature of the photon distribution was increased by the annihilation of positrons and electrons. As this occurred after decoupling, the neutrino temperature was unaffected by this period of annihilation. This lead to a difference in the neutrino and photon temperature, which may be obtained by comparing the effective number of degrees of freedom contributed by relativistic species in thermal equilibrium with photons before and after annihilation. The effective number of relativistic degrees of freedom for particles in thermal equilibrium with photons is given by [38]:

$$g_*^{th}(T) = \sum_{i=b} g_i + \frac{7}{8}\sum_{i=f} g_i \ , \tag{A1}$$

where the species labels b and f refer to bosons and fermions respectively and g is the number of degrees of freedom, $g_b = 2$ and $g_f = 4$. Using Equation (A1) we find:

$$\frac{g_*^{th}(T \gg T_{ann})}{g_*^{th}(T \ll T_{ann})} = \frac{2 + 4(\frac{7}{8})}{2} = \frac{11}{4} \ , \tag{A2}$$

where T_{ann} is the temperature at which the heating of the photons due to the positron-electron annihilation occurs. During positron-electron annihilation, the photon temperature varies as $T_\gamma \propto (g_*^{th})^{-1/3} a^{-1}$, so that after the heating of photons due to positron-electron annihilation the ratio of the cosmic photon and neutrino background temperatures is given by:

$$\frac{T_\nu}{T_\gamma} = \left(\frac{g_*^{th}(T \gg T_{ann})}{g_*^{th}(T \ll T_{ann})}\right)^{1/3} = \left(\frac{4}{11}\right)^{1/3} . \tag{A3}$$

Appendix B: Neutrino Velocity Dispersion

Recall the definition of the velocity dispersion:

$$\begin{aligned} \sigma_v^2 &= \frac{1}{a^2 m^2} < q >^2 \\ &= \frac{1}{a^2\, m^2} \frac{\int_0^\infty q^2 dq q^2 f_0(q)}{\int_0^\infty q^2 dq f_0(q)} \ . \end{aligned} \tag{B1}$$

Recall from Section II B that neutrinos obey the relativistic Fermi-Dirac distribution, Equation (4) as they are relativistic at the time of decoupling. Also recall that after decoupling, the neutrino temperature varies only due to the expansion of the universe, so that aT remains constant and we can use the relation $a(t)T_\nu(t) = a_0 T_{\nu,0}$, where the subscript 0 denotes values today. Using Equation (4), the integral in the denominator can be evaluated as follows:

$$\begin{aligned} \int_0^\infty dq q^4 f_0(q) &= \int_0^\infty dq q^4 \frac{1}{\mathrm{e}^{q/T_0} + 1} \\ &= T_{nu,0}^5 \int_0^\infty dx \frac{x^4}{\mathrm{e}^x + 1} \\ &= T_{nu,0}^5 \frac{45}{2}\zeta(5) \ , \end{aligned} \tag{B2}$$

where the substitution $x = q/T_0$ was made and $\zeta(x)$ is the Riemann zeta function. The integral in the numerator evaluates to:

$$\begin{aligned} \int_0^\infty dq q^2 f_0(q) &= \int_0^\infty dq q^2 \frac{1}{\mathrm{e}^{q/T_0} + 1} \\ &= T_{\nu,0}^3 \int_0^\infty dx \frac{x^2}{\mathrm{e}^x + 1} \\ &= T_{\nu,0}^3 \frac{3}{2}\zeta(3) \ . \end{aligned} \tag{B3}$$

Substituting these integrals into Equation (B1) we find:

$$\sigma_v^2(t) = \frac{1}{a^2(t)\, m_\nu^2} 15 \frac{\zeta(5)}{\zeta(3)} T_{\nu,0}^2 \ . \tag{B4}$$

This is the relation used in the derivation of the neutrino sound speed in Section II B.

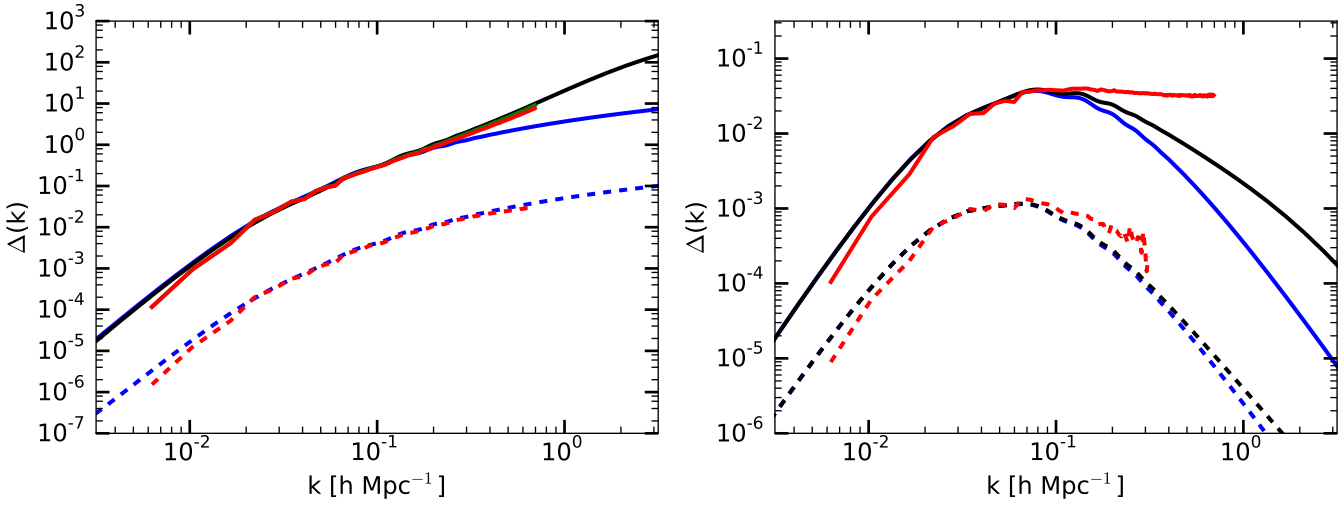

(a) CDM density power spectra

(b) Neutrino density power spectra

Figure 1: The dimensionless CDM (1a) and neutrino (1b) power spectra from the simulations with (red lines) and without (green lines) neutrinos. The CDM power spectra are shown at $z = 0$ (solid lines) and $z = 10$ (dashed lines) while the neutrino power spectra are shown at $z = 0$ (solid lines) and $z = 3$ (dashed lines). The CLASS (blue) and, when they depart from the linear spectra, HALOFIT (black) results are also shown. We do not include results from the simulation without neutrinos at redshift $z = 10$, as neutrinos are added at this redshift and so the two simulations are identical for $z \geq 10$. The CDM power spectrum at $z = 0$ from the simulation including neutrinos lies directly on top of the CDM power spectrum from the simulation without, indicating that for the scales and neutrino mass considered in the simulations, $k < 1$ h Mpc^{-1} and $\sum m_\nu = 0.2$, there is no appreciable effect of massive neutrinos on the CDM power spectrum.

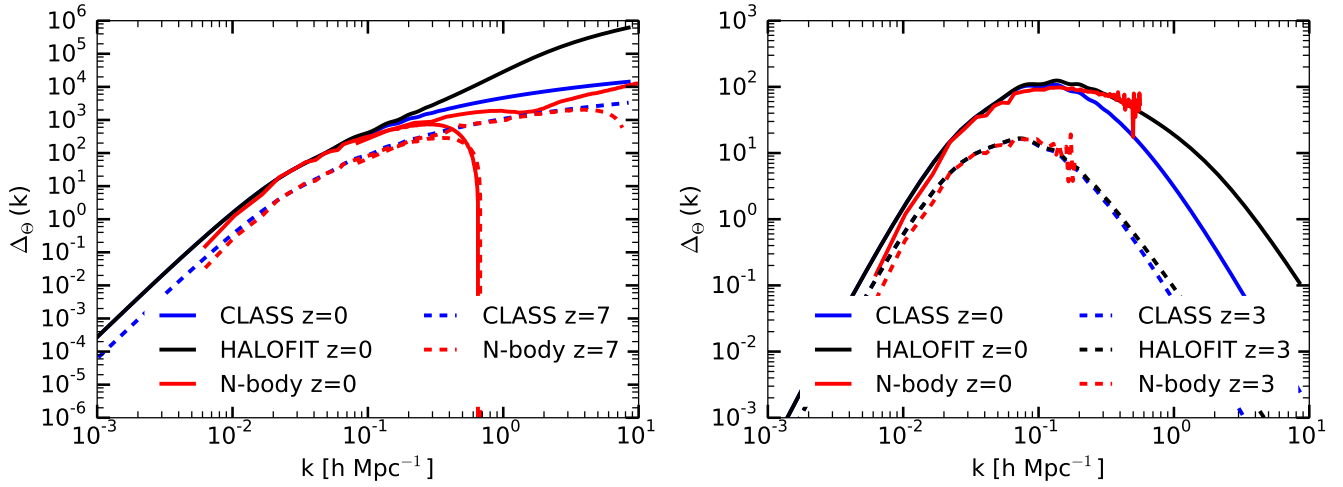

(a) CDM velocity divergence power

(b) Neutrino velocity divergence power

Figure 2: The CDM (2a) and neutrino (2b) velocity divergence power spectra. The numerical CDM power spectra are included from two different simulations with different box sizes. The simulation with the smaller box size is used only for comparison to the semi-linear results, and not for the semi-linear analysis. At $z = 0$, the numerical CDM velocity divergence power is suppressed on small scales compared to linear theory, opposite to what is expected from naively scaling the linear result using HALOFIT. The neutrino velocity divergence power at $z = 0$ is underestimated by linear theory, but agrees well with HALOFIT
.

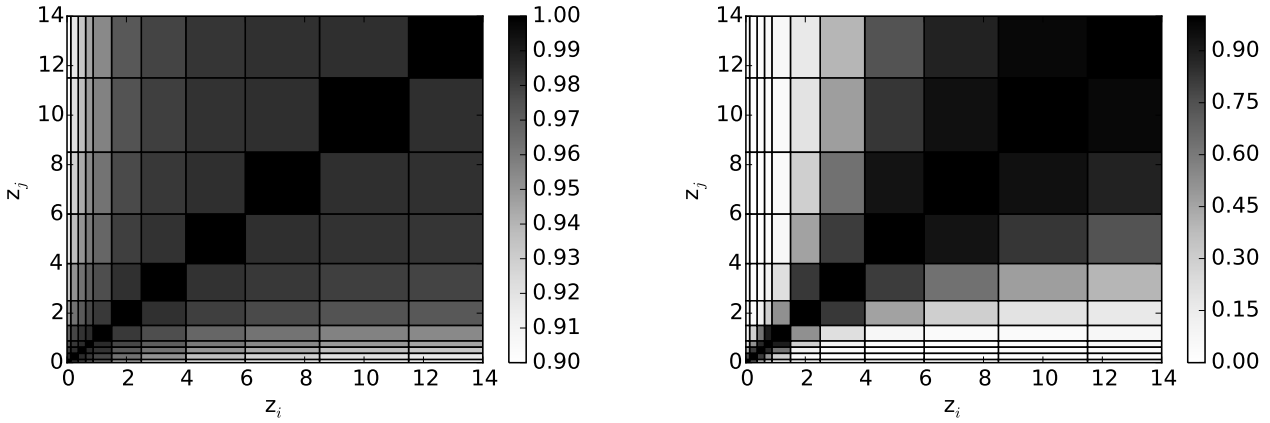

(a) $k = 0.1$ h Mpc^{-1} (b) $k = 1.0$ h Mpc^{-1}

Figure 3: The cross-correlation matrix at $k = 0.1$ h Mpc^{-1} (3a) and $k = 1$ h Mpc^{-1} (3b) when the unequal-time power is calculated among twelve redshifts in the range $z = 0$ to $z = 15$. At $k = 0.1$ h Mpc^{-1}, the cross-correlation coefficients are all close to unity, indicating that the gravitational potential phase changes very little over time at this scale. In contrast, at $k = 1$ h Mpc^{-1}, the cross-correlation coefficients fall to zero rapidly.

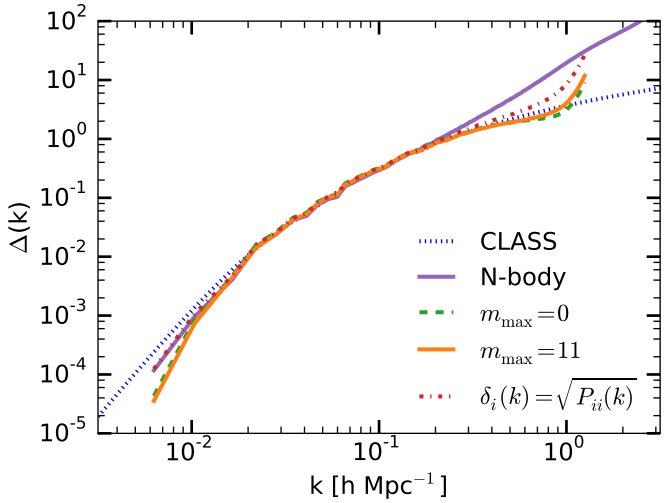

Figure 4: The semi-linear CDM density power spectrum at $z = 0$ along with the spectra from the N-body simulation (solid violet), CLASS (dotted blue), and HALOFIT (dotted teal). The semi-linear power spectrum is calculated with only the primary eigenmode from the decomposition of the cross-correlation matrix (dashed green), with 12 modes (solid orange), and under the assumption that the gravitational potential remains in phase over time (dot-dashed red). The semi-linear power spectra are not a significant improvement upon linear theory.

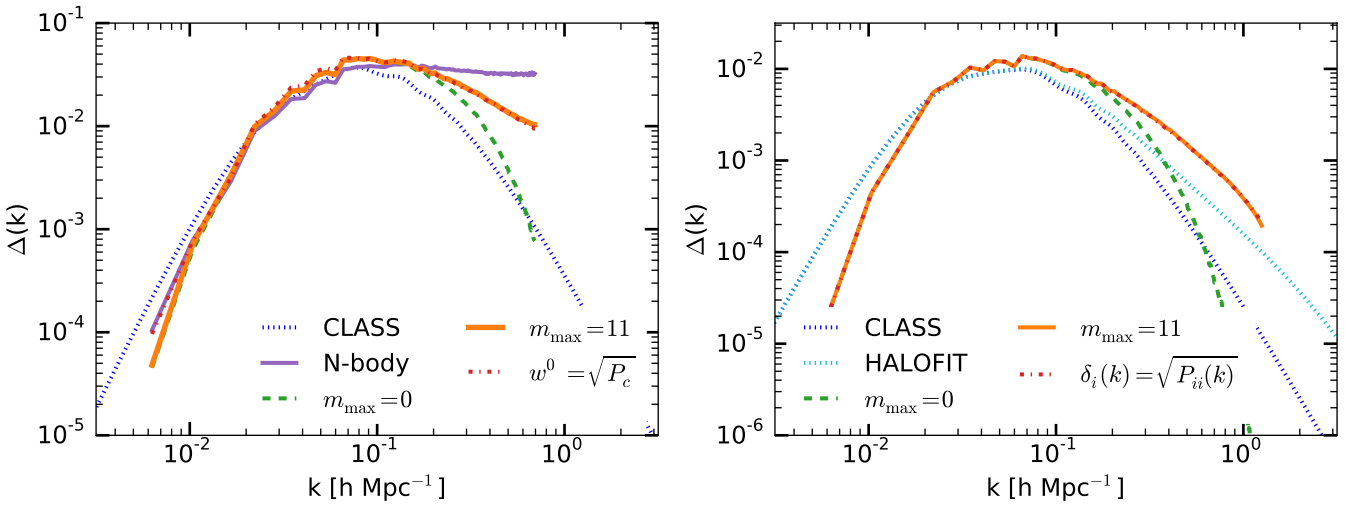

(a) $\sum m_\nu = 0.2$ eV (b) $\sum m_\nu = 0.1$ eV

Figure 5: The semi-linear neutrino density power spectra at $z = 0$ for $\sum m_\nu = 0.2$ eV (5a) and $\sum m_\nu = 0.1$ eV (5b) compared to CLASS (dotted blue), HALOFIT (dotted teal), and the N-body simulation (solid purple). The semi-linear power spectrum is calculated with only the primary eigenmode from the decomposition of the cross-correlation matrix (dashed green), with 12 modes (solid orange), and under the assumption that the gravitational potential remains in phase over time (dot-dashed red). As no simulation was performed with $\sum m_\nu = 0.1$ eV, we have not included numerical results in Figure 5b. The semi-linear method improves upon linear theory and has a higher power than the HALOFIT spectrum on small scales, but does not accurately reproduce the neutrino density power spectrum at $k \gtrsim 0.2$ h Mpc^{-1}. When many modes are included, the results match those obtained by neglecting the changing phase of the gravitational potential.

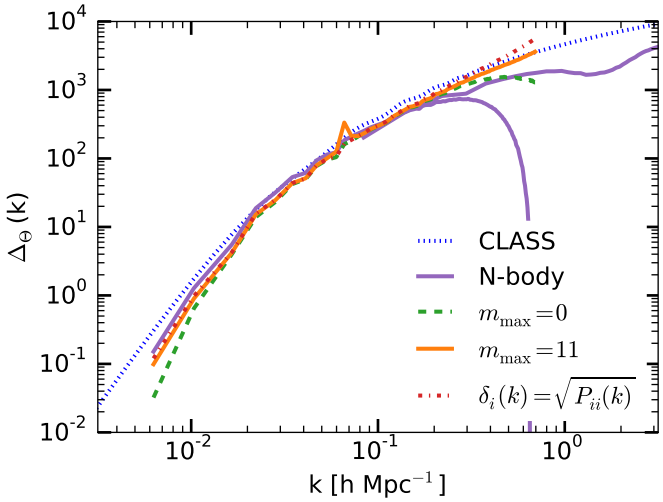

Figure 6: The semi-linear CDM velocity divergence power spectrum at $z = 0$ along with power spectra from the simulation (solid purple) and CLASS (dotted blue). The semi-linear power spectrum is calculated with only the primary eigenmode from the decomposition of the cross-correlation matrix (dashed green), with 12 modes (solid orange), and under the assumption that the gravitational potential remains in phase over time (dot-dashed red). The velocity divergence spectra from two simulations are included for comparison, but only the simulation at smaller wavenumbers was used in the semi-linear method (see Section IV). The semi-linear method provides similar results to linear theory. Including additional modes in the calculation increases the semi-linear power; however the numerical power is decreased on small scales compared to linear theory.

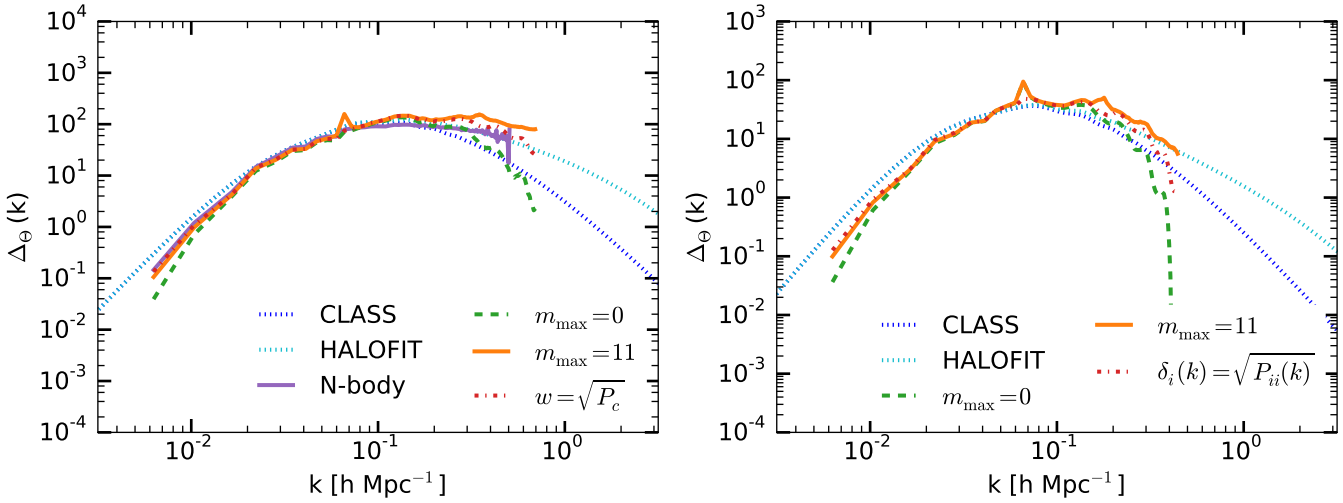

(a) $\sum m_\nu = 0.2$ eV (b) $\sum m_\nu = 0.1$ eV

Figure 7: The semi-linear neutrino velocity divergence power spectrum at $z = 0$ for $\sum m_\nu = 0.2$ eV (7a) and $\sum m_\nu = 0.1$ eV (7b) along with the velocity divergence power spectrum from CLASS (dotted blue), HALOFIT (dotted teal) and the N-body simulation (solid purple). The semi-linear power spectrum is shown when only the primary mode of the cross-correlation matrix is included (dashed green), when 12 modes are included (solid orange), and when the changing phase of the gravitational potential is ignored (dot-dashed red). The numerical spectrum is not shown in Figure 7b as no simulation with $\sum m_\nu = 0.1$ eV was performed. The semi-linear method provides an improvement on linear theory, and traces the HALOFIT and numerical spectra closely.

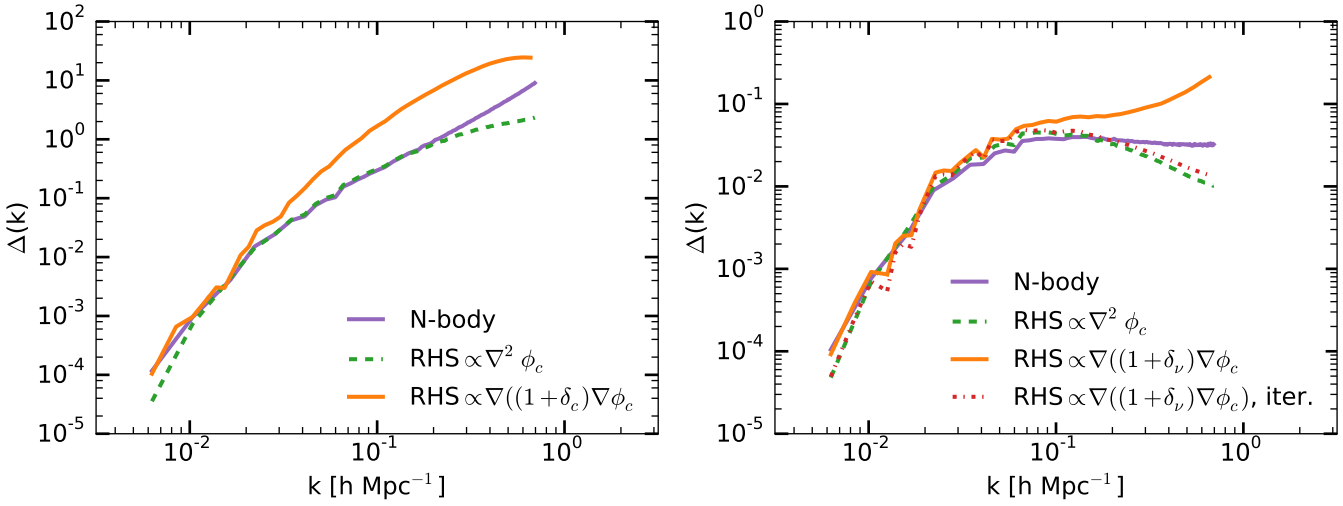

(a) CDM (b) Neutrinos

Figure 8: The CDM (8a) and neutrino (8b) density power spectra calculated from the z-vectors (solid orange), which are computed from the cross-correlation coefficients of $\nabla((1 + \delta_i)\nabla\phi)$ ($i = c, \nu$ for CDM and neutrinos respectively), at $z = 0$ alongside the power spectra from the numerical simulations (solid purple) and from the semi-linear calculation using the w-vectors (dashed green). In Figure 8b, the response to the z-vectors calculated using the iterative method to 4th order (dot-dashed red) is also shown. The power calculated from the z-vectors overestimates the numerical density power for both species.